

MEIOTIC DRIVE

Spindle asymmetry drives non-Mendelian chromosome segregation

Takashi Akera,¹ Lukáš Chmátal,¹ Emily Trimm,¹ Karren Yang,¹ Chant Aonbangkhen,² David M. Chenoweth,² Carsten Janke,^{3,4} Richard M. Schultz,¹ Michael A. Lampson^{1*}

Genetic elements compete for transmission through meiosis, when haploid gametes are created from a diploid parent. Selfish elements can enhance their transmission through a process known as meiotic drive. In female meiosis, selfish elements drive by preferentially attaching to the egg side of the spindle. This implies some asymmetry between the two sides of the spindle, but the molecular mechanisms underlying spindle asymmetry are unknown. Here we found that CDC42 signaling from the cell cortex regulated microtubule tyrosination to induce spindle asymmetry and that non-Mendelian segregation depended on this asymmetry. Cortical CDC42 depends on polarization directed by chromosomes, which are positioned near the cortex to allow the asymmetric cell division. Thus, selfish meiotic drivers exploit the asymmetry inherent in female meiosis to bias their transmission.

Genetic conflict is inherent in any haploid-diploid life cycle because genetic elements compete for transmission through meiosis. Mendel's law of segregation states that alleles of a gene are transmitted with equal probability, but this law can be violated by selfish genetic elements through meiotic drive—for example, by eliminating competing gametes (e.g., sperm killing or spore killing) or by exploiting the asymmetry in female meiosis to increase transmission to the egg. Despite the impact of meiotic

drive on evolution and genetics (1–4), the underlying mechanisms are largely unknown.

Female meiosis provides a clear opportunity for selfish elements to cheat because only chromosomes that segregate to the egg can be transmitted to offspring, whereas the rest are degraded in polar bodies. Conceptually, female meiotic drive depends on three conditions: asymmetry in cell fate, a functional difference between homologous chromosomes that influences their segregation, and asymmetry within the meiotic spindle (5).

The asymmetry in cell fate is well established (6), and chromosomal rearrangements and amplifications of repetitive sequences (e.g., centromeres) are associated with biased segregation (7–10). Asymmetry within the meiotic spindle was noted in grasshopper in 1976 (11) but not studied further.

Oocyte spindles are positioned close to the cortex and oriented perpendicular to the cortex so that cytokinesis produces a large egg and a small polar body. A selfish element drives by preferentially attaching to the egg side of the spindle, implying some difference in microtubules (MTs) between the egg and cortical sides. To determine how such spindle asymmetry is regulated, using mouse oocytes as a model for meiotic drive (10, 12), we tested for asymmetry in posttranslational modifications that functionally diversify MTs (fig. S1A) (13–15). Only tyrosinated (Tyr) and detyrosinated (dTyr) α -tubulin showed asymmetry, with the cortical side enriched for Tyr α -tubulin and the egg side for dTyr α -tubulin (Fig. 1, A and C, and fig. S1B). Furthermore, we found that spindles were asymmetric late in metaphase of meiosis I (MI)

¹Department of Biology, School of Arts and Sciences, University of Pennsylvania, Philadelphia, PA 19104, USA.

²Department of Chemistry, School of Arts and Sciences, University of Pennsylvania, Philadelphia, PA 19104, USA.

³Institut Curie, Paris Sciences & Lettres (PSL) Research University, CNRS UMR3348, Centre Universitaire, Bâtiment 110, F-91405 Orsay, France. ⁴Université Paris Sud, Université Paris-Saclay, CNRS UMR3348, Centre Universitaire, Bâtiment 110, F-91405 Orsay, France.

*Corresponding author. Email: lampson@sas.upenn.edu

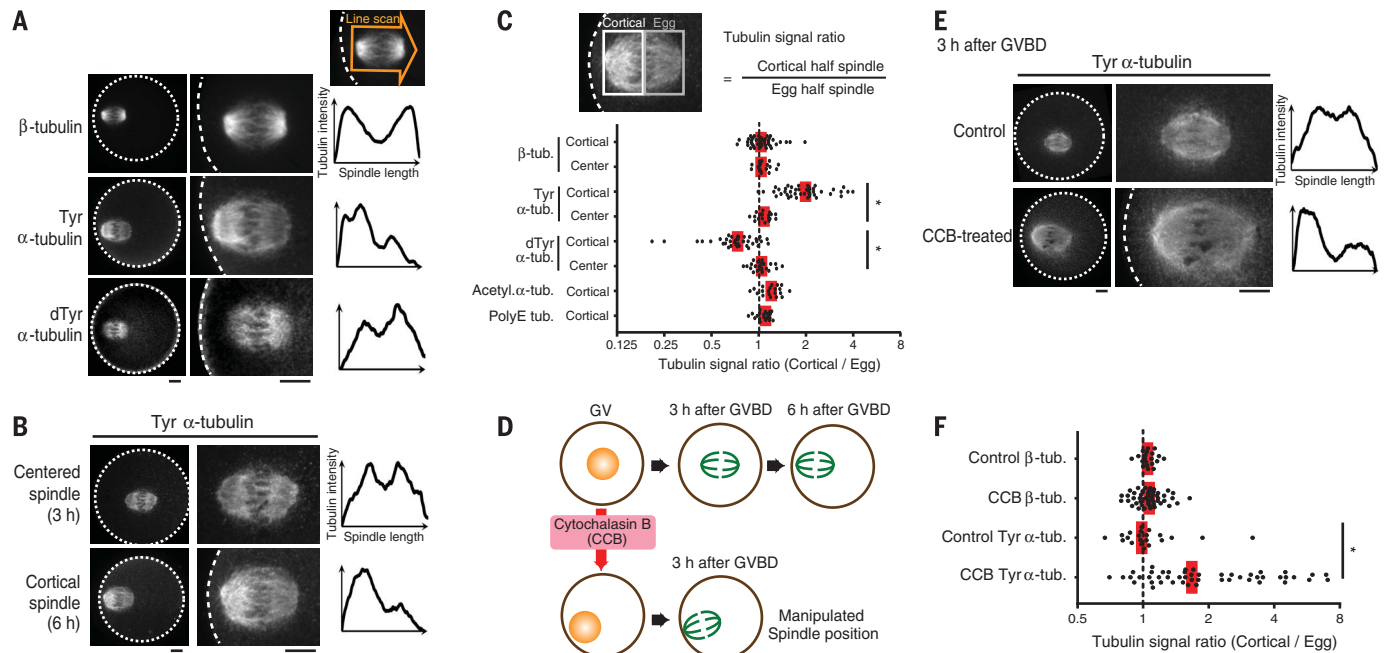


Fig. 1. Cortical proximity induces asymmetry within the mouse oocyte spindle. (A to F) CF-1 oocytes were fixed at metaphase I and stained for the indicated posttranslational modifications on tubulin. Cortical spindles (A) to (C) were examined at 6 hours after GVBD and centered spindles (B) and (C) at 3 hours after GVBD. Cortical spindles in oocytes treated with CCB were examined at 3 hours after GVBD (D) to (F). Images (A), (B), and (E) are sum

intensity z-projections showing the whole oocyte (left) or a magnified view of the spindle (right). Dashed line, cortex; scale bars, 10 μ m. Graphs are line scans of tubulin intensity across the spindle. Spindle asymmetry was quantified (C) and (F) as the ratio of the cortical half to the egg half ($n > 18$ spindles for each condition). In (C), acetylated α -tubulin and polyE tubulin are other posttranslational modifications. Each dot represents a single spindle. Red line, median; * $P < 0.0001$.

when positioned near the cortex, but not earlier when positioned in the center of the oocyte (Fig. 1, B to D, and fig. S2). Because the MI spindle first forms in the center and then migrates toward the cortex (16–20), asymmetry might depend on either cortical proximity or time, or both. To distinguish between these possibilities, we manipulated spindle position by treating oocytes with cytochalasin B (CCB) before maturation to inhibit actin polymerization. The nucleus drifted to the cortex in 24% of these oocytes, with the spindle

positioned near the cortex by 3 hours after germinal vesicle breakdown (GVBD) versus migration at 6 hours under normal conditions (Fig. 1D and fig. S3A). Cortical spindles in CCB-treated oocytes showed asymmetric Tyr α -tubulin staining at 3 hours after GVBD, whereas β -tubulin staining remained symmetric (Fig. 1, E and F, and fig. S3B). Similar results were obtained with cytochalasin D (fig. S3C). Asymmetry could be created if the spindle pole closer to the cortex generated more Tyr α -tubulin. However, misoriented spindles

parallel to the cortex also had stronger Tyr α -tubulin signals on the cortical side, inconsistent with a difference between spindle poles (fig. S4). Thus, the cortex directly regulates MTs to induce asymmetry within the spindle.

The cortex overlying the spindle is polarized through a chromatin-based gradient of guanosine triphosphate-bound RAN (RAN^{GTP}) (21, 22) (fig. S5A) and enriched in multiple signaling factors, including active CDC42 and RAC GTPases, and in polymerized actin (called the actin cap)

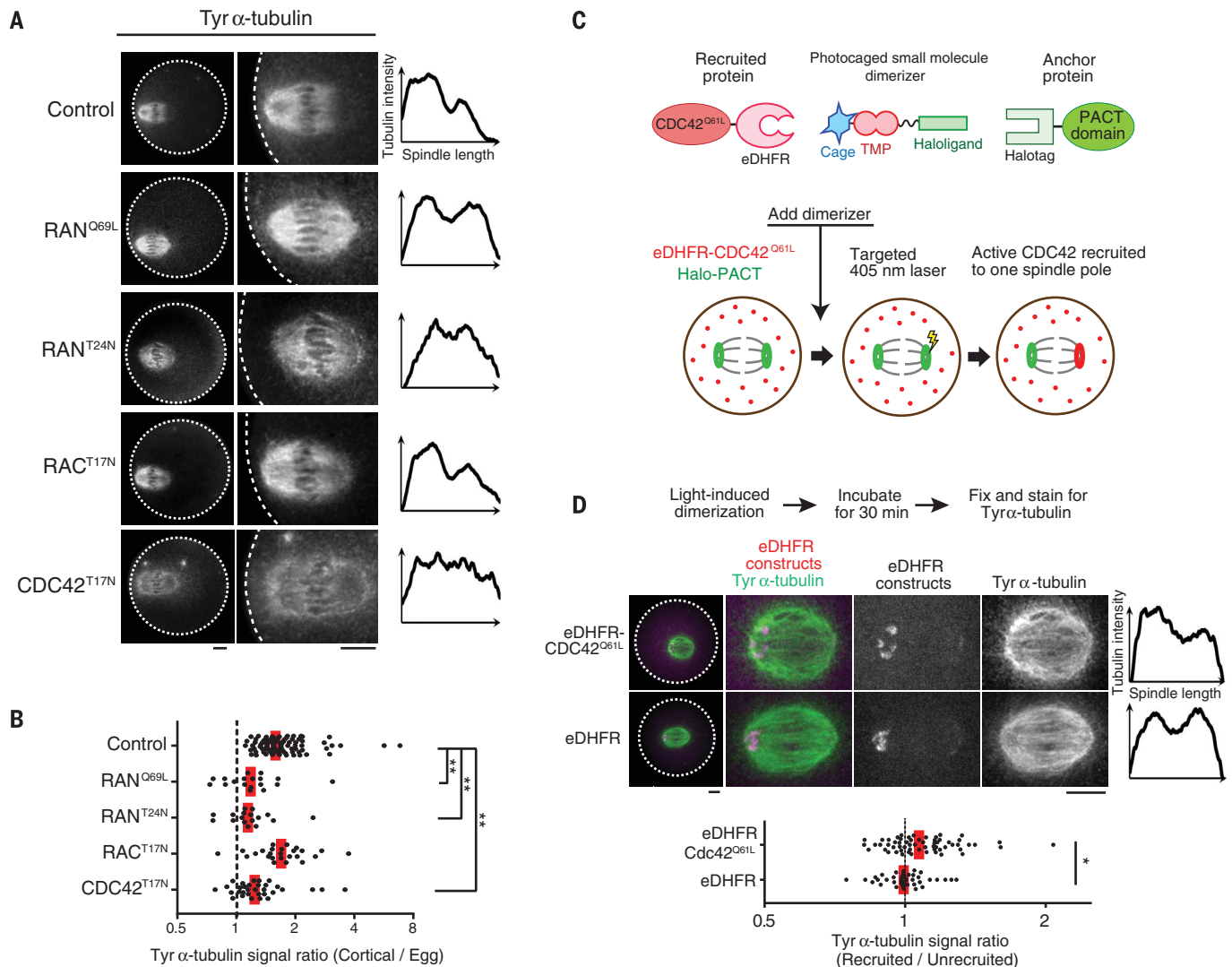


Fig. 2. Cortical polarization and localized CDC42 signaling induce spindle asymmetry. (A and B) CF-1 oocytes expressing the indicated GTPase mutant were fixed 6 hours after GVBD and stained for Tyr α -tubulin. Images are sum intensity z-projections showing the whole oocyte (left) or a magnified view of the spindle (right), and graphs are line scans of tubulin intensity across the spindle. Spindle asymmetry was quantified (B) as the ratio of the cortical half to the egg half ($n > 17$ spindles for each condition). (C) Schematics of the light-induced dimerization experiment. The dimerizer is composed of a HaloTag ligand linked to the eDHFR ligand trimethoprim (TMP), which is photocaged. The PACT domain, fused to enhanced green fluorescent protein (EGFP) and HaloTag, localizes to spindle poles, and CDC42^{Q61L} Δ CAAX is fused to mCherry and eDHFR. The

dimerizer covalently binds Halo-PACT at spindle poles, and eDHFR-CDC42^{Q61L} Δ CAAX is recruited to one pole by local uncaging with light. (D) Halo-EGFP-PACT was coexpressed with either mCherry-eDHFR-CDC42^{Q61L} Δ CAAX (top) or mCherry-eDHFR (bottom) in CF-1 oocytes. Recruitment of eDHFR fusion proteins was induced by uncaging at one spindle pole. Oocytes were fixed and stained for Tyr α -tubulin 30 min after uncaging. Images are maximum intensity z-projections showing whole oocytes (left) or magnified views of the spindle (right), and graphs are line scans of tubulin intensity across the spindle. Spindle asymmetry was quantified as the ratio of the recruited side to the unrecruited side ($n > 39$ spindles for each condition). Each dot represents a single spindle. Red line, median; scale bars, 10 μ m; * $P < 0.01$; ** $P < 0.0001$.

(6, 23, 24) (fig. S5A). To determine whether spindle asymmetry depends on cortical polarization, we expressed either constitutively active (RAN^{Q69L} ; Q, glutamine; L, leucine) or dominant-negative (RAN^{T24N} ; T, threonine; N, asparagine) RAN mutants. In each case, loss of polarization led to loss of spindle asymmetry (Fig. 2, A and B, and fig. S5B). We next tested CDC42 and RAC GTPases by expressing dominant-negative mutants. $\text{CDC42}^{\text{T17N}}$ diminished the Tyr α -tubulin signal overall and prevented asymmetry, whereas RAC^{T17N} did not affect asymmetry (Fig. 2, A and B, and fig. S5, B and C). Furthermore, expressing a constitutively active CDC42 mutant with the plasma membrane-targeting CAAX motif removed ($\text{CDC42}^{\text{Q61L}}\Delta\text{CAAX}$) (25) significantly increased Tyr α -tubulin signal (fig. S7) (CAAX; C, cysteine; A, any aliphatic amino acid residue; X, any amino acid residue). We next tested whether the actin cap, which depends on CDC42 activity (24) (fig. S5A), contributes to spindle asymmetry. Inhibiting the actin-

nucleating actin-related protein 2/3 (Arp2/3) complex with the small-molecule inhibitor CK-666 abolished actin cap formation (26) but did not affect spindle asymmetry (fig. S6). Thus, active CDC42 is sufficient to increase α -tubulin tyrosination and is required for spindle asymmetry independent of actin cap formation.

Our observations suggest that asymmetric localization of active CDC42 relative to the spindle is the mechanism underlying spindle asymmetry. To test this hypothesis, we developed an optogenetic strategy to target active CDC42 to one pole of a centered spindle, which is normally symmetric, using a photocaged small molecule that heterodimerizes HaloTag and *Escherichia coli* dihydrofolate reductase (eDHFR) fusion proteins (27, 28) (Fig. 2C). We used HaloTag fused to a PACT domain, which localizes to spindle poles (29), to recruit eDHFR fusion proteins specifically to one pole by local uncaging of the dimerizer (fig. S8A). Recruiting the constitutively active

$\text{CDC42}^{\text{Q61L}}\Delta\text{CAAX}$ mutant induced spindle asymmetry by increasing Tyr α -tubulin signals on the recruited side, whereas recruiting eDHFR alone had no effect (Fig. 2D and fig. S8B). These results strongly support our model that cortically localized CDC42 activity induces asymmetry within the spindle. Several factors may contribute to the weaker asymmetry induced by our optogenetic approach, compared to that observed normally on spindles near the cortex. $\text{CDC42}^{\text{Q61L}}\Delta\text{CAAX}$ expression increased Tyr α -tubulin overall (fig. S7), leaving less opportunity to create asymmetry by a further increase on one side. In addition, experimentally induced amounts of CDC42 at spindle poles may be lower than normal amounts at the cortex, and other cortical factors may also contribute to the asymmetry.

To determine the importance of spindle asymmetry for meiotic drive, we measured the biased orientation of selfish centromeres toward the egg pole in hybrid oocytes produced in a cross between two mouse strains, CHPO and CF-1. Bivalents in these oocytes have both weaker and stronger centromeres, inherited from CHPO and CF-1 mice, respectively (Fig. 3A). Stronger centromeres have higher amounts of kinetochore proteins and more minor satellite DNA that contains binding sites for the centromere protein CENP-B (10, 12). Using fluorescently tagged CENP-B to distinguish stronger and weaker centromeres in live cells, we showed that stronger centromeres preferentially oriented toward the egg pole just before anaphase I (10) (Fig. 3B, late metaphase I). To abolish spindle asymmetry, which we also observed in this hybrid strain (fig. S9), we expressed RAN^{Q69L} or $\text{CDC42}^{\text{T17N}}$ mutants. Biased orientation was lost in both cases (Fig. 3B), demonstrating that meiotic drive depended on spindle asymmetry induced by cortical polarization.

Initial MT attachments are established before spindle migration to the cortex (30), while the spindle is symmetric, and we did not find biased orientation shortly after migration in CHPO \times CF-1 hybrid oocytes (Fig. 3B, early metaphase I). Thus, the bias arose from reorientation or flipping of stronger centromeres from the cortical to the egg side of the spindle while it was cortically positioned and asymmetric. Hybrid oocytes remained in MI for 2 to 5 hours after spindle migration, likely because of chromosomes positioned off-center on the spindle (12, 31) (Fig. 3B), which would provide time for these flipping events. Indeed, we found examples of bivalents flipping after spindle migration in hybrid oocytes (21 events in 23 cells) (Fig. 4A), consistent with previous observations (30). To establish a bias, flipping must preferentially occur in one direction, which suggests that one orientation is relatively more unstable than the other and implies differences between centromeres of homologous chromosomes and between the two sides of the spindle. To test for these differences in hybrid oocytes, we examined cold-stable kinetochore-MT fibers (32). Stronger centromeres had more unstable attachments compared to weaker centromeres, particularly when facing the cortical side of the spindle (Fig. 4B). Thus, stronger centromeres are more likely to

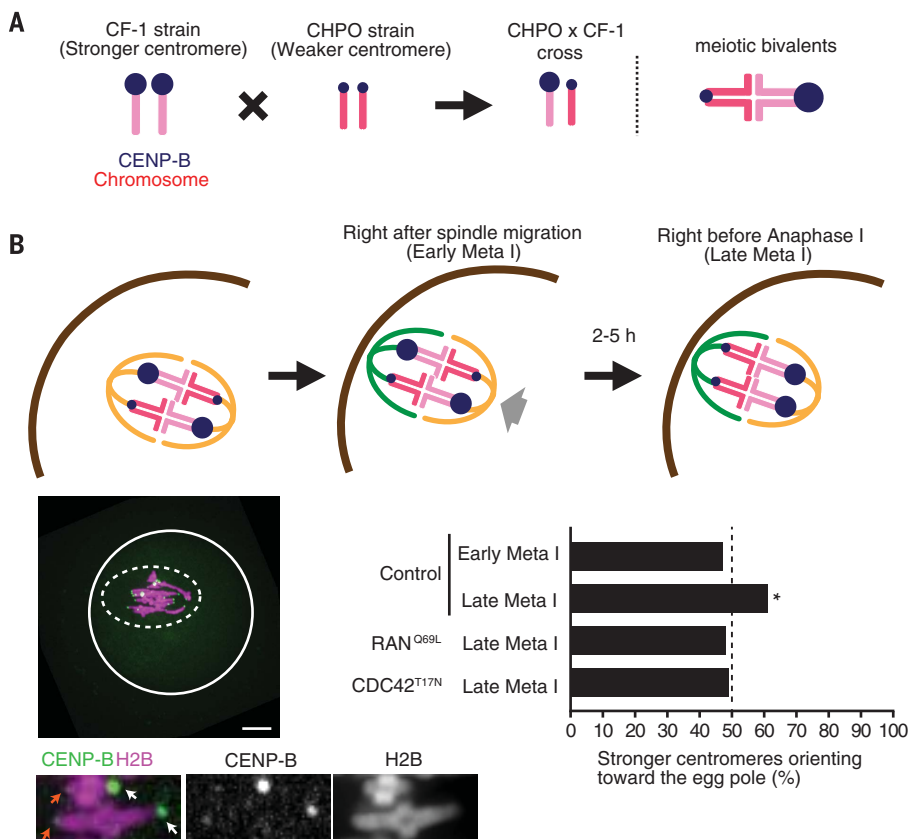


Fig. 3. Spindle asymmetry is essential for biased orientation of selfish centromeres.

(A) Schematic of biased orientation assay. A mouse strain with stronger centromeres (CF-1) is crossed to a strain with weaker centromeres (CHPO). Bivalents in the hybrid offspring contain both stronger and weaker centromeres, which can be distinguished by CENP-B amounts. (B) CHPO \times CF-1 hybrid oocytes expressing CENP-B-EGFP and histone 2B (H2B)-mCherry were imaged live, either shortly after spindle migration to the cortex [within 30 min, early metaphase I (meta I)] or shortly before anaphase onset (within 30 min, late meta I). Image is a maximum intensity z-projection showing late meta I. White line, oocyte cortex; dashed line, spindle outline; scale bar, 10 μm . Bottom images are optical slices showing two bivalents. Arrows indicate stronger (white) and weaker (orange) centromeres. The fraction of bivalents with the stronger centromere oriented toward the egg was quantified; $n = 152$ bivalents for early meta I, 204 for late meta I, 108 for RAN^{Q69L} , and 143 for $\text{CDC42}^{\text{T17N}}$. * $P < 0.005$, indicating significant deviation from 50%.

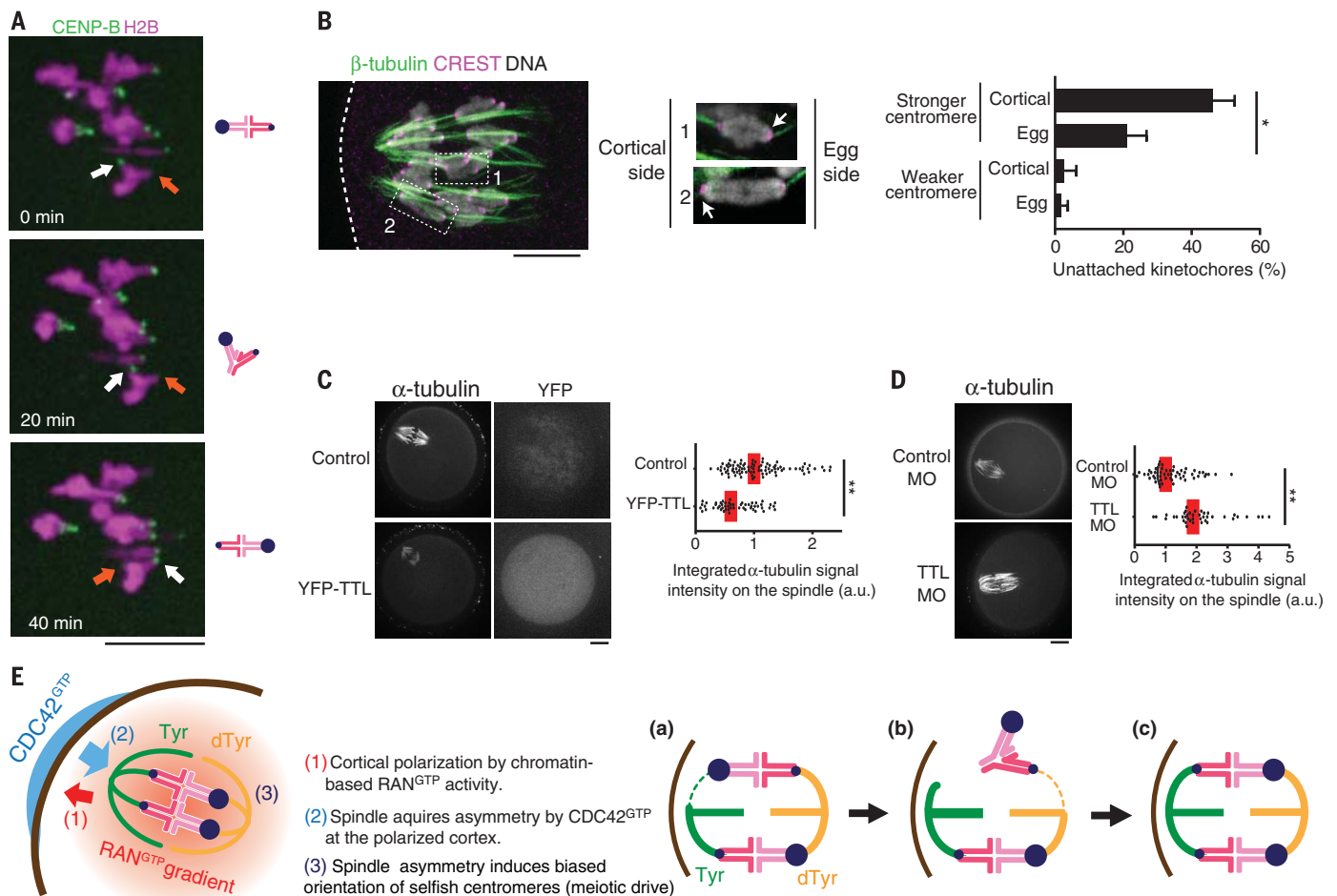


Fig. 4. MT tyrosination promotes unstable interactions between selfish centromeres and the cortical side of the spindle. (A) CHPO \times CF-1 hybrid oocytes expressing CENP-B-mCherry and H2B-EGFP were imaged live after spindle migration to the cortex ($n = 23$ cells). Time-lapse images show an example of bivalent flipping. Arrows indicate stronger (white) and weaker (orange) centromeres. (B) CHPO \times CF-1 hybrid oocytes were analyzed for cold-stable MTs at 8 hours after GVBD. Enlarged images are optical slices showing individual bivalents with the stronger centromere (arrow) either facing the egg side and attached to cold-stable MTs (1) or facing the cortical side and not attached (2). Weaker centromeres are attached in both cases. Graph shows the average percentage of centromeres without cold-stable attachments. Error bars represent SD for three independent experiments (>50 bivalents analyzed in each experiment). $*P < 0.01$. (C and D) CF-1 oocytes expressing yellow

fluorescent protein (YFP)-TTL or microinjected with morpholino (MO) against TTL were analyzed for cold-stable MTs at 6 hours after GVBD. Graphs show integrated α -tubulin intensity in the spindle ($n > 41$ spindles for each condition). Each dot represents a single spindle. Red line, median; a.u., arbitrary units; $*P < 0.001$. Images (A) to (D) are maximum intensity z-projections. Scale bars, 10 μ m. (E) Model for spindle asymmetry and meiotic drive. Left, cortical signals regulate MTs to induce tyrosination asymmetry within the spindle, and stronger centromeres (larger blue circles) orient preferentially to the egg side. Right, bivalent orientation is initially random (a), but attachment of a stronger centromere to the cortical side is unstable and tends to detach (b), which is followed by detachment of the weaker centromere, likely owing to loss of tension across the bivalent, and reorientation. This biased flipping of stronger centromeres to the egg side leads to biased orientation (c).

detach, and the cortical side is more susceptible to detachment. To test whether the enrichment of Tyr α -tubulin makes the cortical side more unstable, we modulated the expression of tubulin tyrosine ligase (TTL), which catalyzes α -tubulin tyrosination (33). TTL overexpression increased Tyr α -tubulin and destabilized spindle MTs on the basis of sensitivity to low temperature (34), whereas depleting TTL decreased Tyr α -tubulin and stabilized spindle MTs (Fig. 4, C and D, and fig. S10, A and B). Thus, Tyr α -tubulin asymmetry allows stronger centromeres to interact differentially with the two sides of the spindle to preferentially orient toward the egg pole (Fig. 4E).

Here we have shown that asymmetry within the spindle is essential for meiotic drive. Because signals from the cell cortex regulate MTs to induce spindle asymmetry and the cortical side ultimately ends up in the polar body, our findings explain how spindle asymmetry is consistently oriented relative to cell fate, providing spatial cues to guide the segregation of selfish elements. Moreover, the cortical signals are a product of polarization directed by chromosomes positioned near the cortex. This chromosome positioning is crucial for female meiosis because it allows the highly asymmetric division that is a universal feature of sexual reproduction in animals (6, 21, 23, 35). Thus, selfish

drive elements exploit the asymmetry inherent in female meiosis to bias their chances of transmission to the next generation.

REFERENCES AND NOTES

1. J. H. Werren, *Proc. Natl. Acad. Sci. U.S.A.* **108**, 10863–10870 (2011).
2. W. R. Rice, *Annu. Rev. Ecol. Evol. Syst.* **44**, 217–237 (2013).
3. A. K. Lindholm *et al.*, *Trends Ecol. Evol.* **31**, 315–326 (2016).
4. Q. Helleu, P. R. Gérard, C. Montchamp-Moreau, *Cold Spring Harb. Perspect. Biol.* **7**, a017616 (2014).
5. F. Pardo-Manuel de Villena, C. Sapienza, *Mamm. Genome* **12**, 331–339 (2001).
6. R. Li, D. F. Albertini, *Nat. Rev. Mol. Cell Biol.* **14**, 141–152 (2013).
7. J. P. Didion *et al.*, *PLOS Genet.* **11**, e1004850 (2015).

8. L. Fishman, A. Saunders, *Science* **322**, 1559–1562 (2008).
9. F. Pardo-Manuel de Villena, C. Sapienza, *Genetics* **159**, 1179–1189 (2001).
10. A. Iwata-Otsubo *et al.*, *Curr. Biol.* **27**, 2365–2373.e8 (2017).
11. G. M. Hewitt, *Chromosoma* **56**, 381–391 (1976).
12. L. Chmátal *et al.*, *Curr. Biol.* **24**, 2295–2300 (2014).
13. P. Robison *et al.*, *Science* **352**, aaf0659 (2016).
14. M. Barisic *et al.*, *Science* **348**, 799–803 (2015).
15. C. Janke, *J. Cell Biol.* **206**, 461–472 (2014).
16. J. Azoury, K. W. Lee, V. Georget, P. Hikal, M.-H. Verlhac, *Development* **138**, 2903–2908 (2011).
17. M. Almonacid, M.-É. Terret, M.-H. Verlhac, *J. Cell Sci.* **127**, 477–483 (2014).
18. M. Schuh, J. Ellenberg, *Curr. Biol.* **18**, 1986–1992 (2008).
19. K. Yi *et al.*, *J. Cell Biol.* **200**, 567–576 (2013).
20. J. Azoury *et al.*, *Curr. Biol.* **18**, 1514–1519 (2008).
21. M. Deng, P. Suraneni, R. M. Schultz, R. Li, *Dev. Cell* **12**, 301–308 (2007).
22. B. Dehapiot, G. Halet, *Cell Cycle* **12**, 1672–1678 (2013).
23. G. Halet, J. Carroll, *Dev. Cell* **12**, 309–317 (2007).
24. B. Dehapiot, V. Carrière, J. Carroll, G. Halet, *Dev. Biol.* **377**, 202–212 (2013).
25. I. M. Ahearn, K. Haigis, D. Bar-Sagi, M. R. Philips, *Nat. Rev. Mol. Cell Biol.* **13**, 39–51 (2011).
26. K. Yi *et al.*, *Nat. Cell Biol.* **13**, 1252–1258 (2011).
27. E. R. Ballister, C. Aonbangkhen, A. M. Mayo, M. A. Lampson, D. M. Chenoweth, *Nat. Commun.* **5**, 5475 (2014).
28. H. Zhang *et al.*, *Nat. Chem. Biol.* **13**, 1096–1101 (2017).
29. A. K. Gillingham, S. Munro, *EMBO Rep.* **1**, 524–529 (2000).
30. T. S. Kitajima, M. Ohsugi, J. Ellenberg, *Cell* **146**, 568–581 (2011).
31. L. Chmátal, K. Yang, R. M. Schultz, M. A. Lampson, *Curr. Biol.* **25**, 1835–1841 (2015).
32. C. L. Rieder, *Chromosoma* **84**, 145–158 (1981).
33. A. E. Prota *et al.*, *J. Cell Biol.* **200**, 259–270 (2013).
34. S. Inoué, H. Sato, *J. Gen. Physiol.* **50**, 259–292 (1967).
35. R. Gorelick, J. Carpinone, L. J. Derrough, *Biol. J. Linn. Soc. London* **120**, 1–21 (2016).

ACKNOWLEDGMENTS

We thank B. E. Black and M. T. Levine for comments on the manuscript, G. Halet for the CDC42 and RAC constructs and

discussions, R. Li for the RAN constructs, and B. L. Prosser for the dTyr α -tubulin and TTL antibodies. The research was supported by NIH grants GM107086 (M.A.L. and R.M.S.) and GM122475 (M.A.L.); by Institut Curie, CNRS, ANR-10-LBX-0038 part of the IDEX Idex PSL ANR-10-IDEX-0001-02 PSL, and by the grant INCA_6517 (C.J.); and by a Japan Society for the Promotion of Science postdoctoral fellowship for research abroad and a research fellowship from Uehara Memorial Foundation (T.A.). Data described can be found in the main figures and supplementary materials. The authors declare no conflict of interests.

SUPPLEMENTARY MATERIALS

www.sciencemag.org/content/358/6363/668/suppl/DC1

Materials and Methods

Figs. S1 to S10

References (36–38)

17 February 2017; resubmitted 10 August 2017

Accepted 20 September 2017

10.1126/science.aan0092